MICROPOROUS COMPOSITE SiO_2-TiO_2 SPHERES PREPARED VIA THE PEROXO ROUTE: LEAD(II) REMOVAL IN AQUEOUS MEDIA

Roman Morozov[1], Igor Krivtsov[1,2], Viacheslav Avdin[1], Zakariae Amghouz[3], Alexander Gorshkov[1], Ekaterina Pushkova[1], Oleg Bol'shakov[1], Aleksandra Bulanova[1], Marina Ilkaeva[2]*

(1) Department of Chemistry, South Ural State University, 454080 Chelyabinsk, Russia.

(2) Departments of Organic and Inorganic Chemistry and Physical and Analytical Chemistry, University of Oviedo-CINN, 33006 Oviedo, Spain.

(3) Department of Materials Science and Metallurgical Engineering, University of Oviedo, Campus Universitario, 33203 Gijón, Spain.

**Corresponding author E-mail: uo247495@uniovi.es; Tel: +34 985 103 00*

Abstract

Composite microporous SiO_2-TiO_2 spheres and micro/mesoporous TiO_2 spheres were prepared via the template-free two-step synthetic route using aqueous peroxotitanate solution and tetraethyl orthtosilicate (TEOS) as precursors. Both the composite SiO_2-TiO_2 and pure TiO_2 spheres prepared by the solvent-exchange method were initially non-porous, but the applied reflux treatment in water-ethanol suspension successfully transformed them into microporous materials with high apparent surface areas approaching 500 $m^2 \cdot g^{-1}$ and the micropore volume of 0.17 $cm^3 \cdot g^{-1}$, while maintaining the same morphology. The prepared composites retained high values of pore volume and specific surface area up to 400 ºC of thermal treatment temperature. The crystallization of TiO_2 into the anatase phase in the mixed oxide occurred only at 700 ºC, that process was also accompanied by the significant reduction of pore volume, as well as apparent surface area values. Both synthesized composite oxides and pure titania were tested, in aqueous

media, on the lead(II) removal; they demonstrated high adsorption capacities, reaching 340 mg(Pb^{2+})·g^{-1}. Moreover, the mixed silica-titania oxide was found to be more efficient adsorbent at low pH values.

Keywords: SiO_2, TiO_2, spherical particles, silica-titania, microporous, lead adsorption, peroxo method.

1 Introduction

Silica- and titania-based functional materials are frequently used for various environmental applications due to their high chemical stability, non-toxicity and low cost. It is a common notion that the formation of silica-titania composites might significantly modify and improve some properties of the constituents, widening the application range of these materials [1-10]. This occurs because of the Si–O–Ti linkages formation in the bulk and on the surface of the mixed oxide, creation of tetracoordinated titanium fragments, and stabilization of titania in an amorphous state. The acidity arising from the above mentioned structural changes makes SiO_2-TiO_2 an interesting active material for various catalytic processes [1-3,10-12]. However, the preparation of a molecularly homogeneous silica-titania composite via sol-gel or precipitation routes meets with obstacles. Titanium has significantly larger partial positive charge than silicon, which makes it very reactive in the presence of water, thus tending to form hydrous titania. Thus, certain measures preventing the separation of the two oxides implying the use of anhydrous organic solvents [13], complexing agents [14], or pre-hydrolysis of the less reactive silica precursor [15] are commonly applied. Obviously, the control of hydrolysis and condensation rates of titanium oxo-hydroxo complexes and their interaction with silica species is even more complicated in aqueous medium. The means of manipulating the Ti-precursors hydrolysis rates and molecular homogeneity in water-born systems generally include the use of carboxylic acids [16] and amines [17] as complexing agents.

Other important aspects of silica-titania properties determining the performance in catalytic reactions and as catalytic supports are morphology, specific surface area (SSA), and porous structure. Spherical morphology is a very convenient form of the particles used as catalysts and adsorbents because it provides dense and uniform packing and favours establishing a laminar flow in such processes as catalysis [1-3], gases separation [4-7], and adsorption[18-21]. Though the methods for spherical SiO_2 fabrication via the Stöber process [22] and for TiO_2 using inorganic and structure-directed routes [23] are well-known, the

reports on the preparation of silica-titania spheres with a high degree of the SiO_2 and TiO_2 mutual mixing are scarce. The porous structure of such composites is a key feature for many applications. Microporosity provides accessibility for small molecules and ions to the active sites of silica, titania and mixed silica-titania materials making them useful in membrane separation technologies [4-7,24] and cation exchange [25,26].

The possibility of application of inorganic materials for adsorption of toxic metal cations from water by adsorption and ion exchange attracts significant interest. Among the variety of heavy metal pollutants found in waste and drinking water, the presence of lead is especially worrying. Water-soluble lead(II) acetate and volatile tetraethyl lead, often encountered in industry, are extremely harmful to humans and environment. Microporous TiO_2 and SiO_2-TiO_2 metal oxides demonstrate higher efficiency in lead uptake from water solutions than the widespread organic polymeric resins [27] or carbon-based adsorbents [28], moreover, their superior chemical and thermal stability make them more promising for long-term application.

Earlier, we described the template-free preparation of homogeneous silica-titania spherical particles with controlled particle sizes [29]. However, low SSA and non-porous nature made their use impossible in many processes. Here, we report the surface activation procedure able to convert non-porous silica-titania spheres into highly microporous solids. Moreover, in this study we address the possible application of both titania and silica-titania materials for Pb^{2+} removal.

2 Experimental

2.1 Chemicals

Titanium oxysulfate hydrate ($TiOSO_4 \cdot H_2O$) containing 17% of H_2SO_4 used as titania source was provided by Alfa Aesar. TEOS (tetraethyloetosilicate) of analytical grade produced by Reachim was used as the precursor for silica. Aqueous ammonia ($NH_3 \cdot H_2O$) solution of 25 wt%, HCl(aq), *n*-propanol, H_2O_2, $(CH_3COO)_2Pb$ (analytical grade), 2,7-bis(2-arsonophenylazo)-1,8-dihydroxynaphthalene-3,6-disulfonic acid (Arsenazo III), acetic acid, and CH_3COONa were of analytical grade and were also produced by Reachim.

2.2 Synthesis of nonporous silica-titania spheres

Preparation of the composite SiO_2-TiO_2 spheres was performed according to the peroxo-mediated solvent exchange route reported in [29,30]. For the synthesis, 2.4 g of titanium oxysulfate (containing 10 mmol of TiO_2) was dissolved in 20-30 mL of deionized water at room temperature and immediately 10 mL of ammonia solution was added to it leading to the formation of white colloidal precipitate. The suspension was thoroughly mixed to ensure complete precipitation of hydrous titania, centrifuged and washed 6 times with deionized water, in order to remove sulfate and ammonium ions. The washed precipitate was placed in an ice bath and 10 mL of H_2O_2 was dropwise added to it, while the suspension was vigorously stirred. Eventually, the complete dissolution of the colloidal precipitate occurred and a transparent yellow solution of titanium peroxo complex was formed. The volume of the titanium peroxo complex solution was adjusted to 100 mL with deionized water and its pH was set to 9.5 by ammonia addition.

Separately, 2.2 mL of TEOS was dissolved in 97.8 mL of *n*-propanol. The choice of the solvent was based on the previous work [29]. The solution of TEOS in *n*-propanol was magnetically stirred for a few minutes and then poured into the aqueous titanium peroxo complex. The mixture turned turbid instantaneously and was left stirring for 24 h. Subsequently, the suspension was centrifuged, washed 6 times with deionized water and dried under vacuum at 50 ºC for 6 h.

For the preparation of pure TiO_2 no TEOS solution was used, instead 100 mL of *n*-propanol was directly poured into the peroxotitanate water solution while magnetically stirred, after 24 h of mixing, the precipitate was washed and dried according to the procedure described in [31].

Pure SiO_2 was synthesized following the same protocol, but in absence of TiO_2 source.

2.3 Surface area activation of the prepared spheres

The silica-titania spherical particles prepared via the method described above were nonporous [29]. In order to modify their porous characteristics, the surface area activation procedure reported earlier for pure TiO_2 spherical particles [31] was implemented. The activation was performed by a post-synthetic treatment in the following way: freshly prepared nonporous silica-titania spheres were suspended in 50 mL of water-ethanol mixture (1:1 ratio by volume) at the pH value of 5, which was set by addition of HCl (1 M). The

suspension was refluxed for 21 h and then the solid phase was separated by centrifugation at 3000 rpm, washed with deionized water and dried at 50 ºC for 24 h. The silica-titania samples prepared in this way were designated as ST50, the same materials calcined at 400 ºC and 700 ºC in air for 1 h were marked ST400 and ST700, respectively. The titania spheres prepared using the same procedure were designated as T50, T400, and T700 depending on the calcination conditions they underwent. Process of surface area enhancement of pure SiO_2 was totally similar to that of the TiO_2 and the SiO_2-TiO_2 composite.

2.4 Characterization

Morphological investigation of the prepared composite silica-titania spheres was performed by a field emission scanning electron microscope (SEM) JEOL JSM 7001F. The SSA, volume and size distribution of micro- and mesopores were probed by N_2 adsorption at 77 K using an ASAP 2020 Micromeritics analyzer. The as-prepared samples were outgassed at 100 ºC for 2 h, while the samples calcined at 400 ºC and 700ºC were outgassed for 2 h at 300 ºC. The XRD patterns were recorded on a Rigaku Ultima IV diffractometer operating at Cu Kα radiation (λ = 0.154 nm). The mean size of anatase crystals was calculated by Scherrer equation for (101) reflection of anatase phase. Thermoanalytical studies were performed using a simultaneous TG-DSC thermal analyzer Netzsch 449 F1 in the temperature range from 25 to 1000 ºC in air flow at the heating rate of 10 ºC·min^{-1}. A Jeol JEM-2100F transmission electron microscope (TEM) equipped with a field emission gun (FEG) was applied for TEM observations. Sample preparation involved dispersion in ethanol, sonication and deposition on a holey carbon film-coated copper grid with subsequent drying, a Gatan SOLARUS 950 was used before investigation. X-ray photoelectron spectroscopy (XPS) analysis was carried out on a SPECS system equipped with a Hemispherical Phoibos analyzer operating at Mg-Kα radiation ($h \cdot \upsilon$ = 1253.6 eV). The FTIR spectra were collected using a Shimadzu IR Affinity spectrometer. The point of zero charge (PZC) of pure titania and silica-titania spheres was measured by a Zetasizer Nano ZS90.

2.5 Lead adsorption experiment

Adsorption of Pb^{2+} ions was studied under isothermal conditions at 25 ºC. Kinetic study of Pb^{2+} ion adsorption was carried out in the following way: to 50 mL of the 500 mg(Pb^{2+})·L^{-1} solution of lead(II) acetate 20 mg of adsorbent was added and the suspension was left shaking. The probes were withdrawn at fixed time intervals and the concentration of lead ions was measured photometrically.

For adsorption isotherm measurement, 25 mL of lead(II) acetate solutions with concentrations of 10, 25, 50, 100, 150, 200, 300, 400 and 500 mg(Pb^{2+})·L^{-1} were placed into glass beakers containing 10 mg of adsorbent and shakes for 1 h. No buffer solution was added and the pH value of the resulted suspensions was found to be equal to 5. In a separate experiment, intending to establish the effect of pH on adsorption capacity, diluted HNO_3 was added to the suspension of lead acetate solution and adsorbent and pH values were set to 1, 2, 3, and 4. After 1 h of shaking, the suspension was centrifuged and Pb^{2+} concentration was measured.

The concentration of Pb^{2+} ions was determined by the photometric method measuring the light absorption of coloured Pb^{2+}complex with Arsenazo III indicator in acetic acid buffer solution having pH 4.8 with the use of a Shimadzu UV 2700 spectrophotometer. The acetic acid buffer solution was prepared by dissolving 3.7 g of CH_3COONa and 1.31 mL of glacial acetic acid in 250 mL of deionized water. The Arsenazo III water solution (0.4 mM) was prepared by dissolving 31 mg of the indicator in 100 mL of deionized water. Calibration curve was built using the set of lead(II) acetate solutions with known concentrations, and it had the correlation coefficient of 0.999. At least three replicate analyses were done for each sample. Adsorption capacity was calculated according to the following equation:

$$Q_{eq} = (C_0 - C_{eq}) * \frac{V}{m} \quad (1),$$

where Q_{eq} is the Pb^{2+} adsorption capacity at equilibrium concentration (in mg·g^{-1}), C_o is the initial Pb^{2+} concentration in lead acetate solution (mg·L^{-1}), C_{eq} is the Pb^{2+} equilibrium concentration (mg·L^{-1}), V is the aliquot volume (L), and M is the mass of the adsorbent (g).

The obtained values were used to calculate the maximum adsorption capacities of the adsorbents in accordance with the Langmuir isotherm model. The linearized form of this model was described by the following equation:

$$\frac{C_{eq}}{Q_{eq}} = \frac{C_{eq}}{Q_m} + \frac{1}{K*Q_m} \quad (2),$$

where Q_m (in $mg \cdot g^{-1}$) is the monolayer capacity (maximum adsorption capacity), and K is the Langmuir equilibrium constant.

$$R_L = \frac{1}{1+K*C_{eq}} \quad (3),$$

where R_L is the dimensionless constant of separation factor.

The Freundlich empirical model was also used for approximation of the adsorption data. Freundlich isotherm was described by the following linearized equation:

$$\ln(Q_{eq}) = \ln(Kf) + \frac{1}{n} * \ln(C_{eq}) \quad (4),$$

where Kf ($(mg\ g^{-1})(L\ mg^{-1})^{1/n}$) is the Freundlich adsorption capacity while lead concentration is 1M, and *n* is a constant which estimates the possibility of adsorption process.

Regeneration experiments were carried out under the same conditions with the concentration of sorbate solution of 500 $mg(Pb^{2+}) \cdot L^{-1}$. In order to regenerate the adsorbents, 0.1 M EDTA solution was applied. After the adsorption cycle the sorbent was put into a glass beaker with 25 mL of EDTA solution and shaken for 30 min. Then the regenerated sample was washed two times with distilled water before using it in the subsequent adsorption cycle.

3 Results and discussion

3.1 Morphology and textural properties

Expectedly, pure SiO_2 prepared via the Stöber-like procedure and underwent the post-synthetic treatment is found in the form of spherical particles with the mean size of 400 nm (see Supplementary Information Fig. S1). The composite silica-titania spheres maintain spherical morphology after being subjected to the post-synthetic treatment, which was intended to enhance their SSA. Comparison of particle sizes of the porous pure TiO_2 (Fig. 1a) and the silica-titania spheres (Fig. 1b) shows significantly larger diameter of the latter, which might be explained by different mechanisms of their formation. Attention is drawn to the fact that the surface of the post-synthetically treated silica-titania spheres (unlike that of the pure TiO_2) does not show any noticeable roughness, probably indicating smaller pore sizes of the composite material.

In earlier works, we reported the preparation of titania [31] and silica-titania [29] spheres by the solvent-exchange method. The as-prepared materials were nonporous [29,31], however, the post-synthetic treatment proposed in [31] allowed to successfully convert nonporous TiO_2 spherical particles into highly mesoporous material. In a similar manner, the apparent SSA of the SiO_2 spheres is greatly enhanced up to 361 m^2g^{-1} after undergoing the proposed post-synthetic treatment converting them into highly microporous material (Fig. S2) The SSA activation procedure applied to the silica-titania composite of the same morphology enhances apparent SSA up to 400-500 $m^2 \cdot g^{-1}$, although the textural properties that the composite material possesses are very different from those of its pure TiO_2 counterpart and resemble pure SiO_2 (Table 1, Fig. 2). According to IUPAC classification [32], the T50 spheres after the surface area activation exhibit the isotherm of mixed I and IV types (Fig. S3), which indicates that this material has a large volume of both micro- and mesopores (Table S1). After calcination at 400 ºC the pure titania loses the volume of its micropores, and its isotherm transforms into type IV (Fig. S3). The presence of micropores in the T50 and T400 samples is explained by high percentage of amorphous phase they contain. The micropores disappear as soon as the thermal treatment temperature is sufficient to completely convert amorphous TiO_2 into crystalline anatase phase (Fig. S3). Finally, the isotherms of the T700 sample acquire type IV, where the mesopores are attributed to the intercrystal voids within the spherical particles (Fig. S3). Nitrogen physisorption by the ST50 and ST400 samples results in the isotherms of type I, according to IUPAC classification (Fig. 2). This isotherm type is a typical of microporous solids. The post-synthetic

treatment helps to increase apparent SSA of the composite oxide by 30 times from 16 $m^2 \cdot g^{-1}$, obtained for the nonporous composite [29], to 503 $m^2 \cdot g^{-1}$ (Table 1). Calcination of the composite at 400 ºC does not destroy its microporous structure, and ST400 shows almost the same value of apparent SSA as does the ST50 sample. Thermal treatment of porous silica-titania at 700 ºC makes it lose nearly all micropores, which is likely to be due to crystallization of TiO_2, leading to the ST700 isotherm of type II, characteristic of nonporous or macroporous solids (Fig. 2). The absence of a hysteresis loop indicates that no mesopores are found in this solid.

Analysis of pore-size distribution reveals an important difference between the porous TiO_2 and the porous SiO_2-TiO_2 samples. Though the pure as-prepared titania also possesses high micropore volume, it loses its high SSA and pore volume while thermally treated (Fig. S4). The composite oxide retains high SSA and micropore volume up to 400 ºC, which is the consequence of the stabilization of the amorphous titania phase inside the silica matrix. The mean micropore size of all the studied samples lies in the region of 0.5 nm (Fig. 3). In order to properly evaluate porous properties of the materials different models are applied. Micropore volumes of the pure titania and the composites are estimated by Dubinin-Astakhov equation (Tables 1 and S1). Size distribution of micropores calculated by the Horwath-Kawazoe model is in the range 3.6-20.0 Å, supposing that the shape of the micropores is spherical (Figs. 3 and S4). External surface area, that is the area calculated excluding micropore surface, is determined by the T-plot approach at relative pressures 0.4-0.6, clearly demonstrating the dominant contribution of micropore SSA to the apparent SSA BET values (Tables 1 and S1).

The nitrogen physisorption study suggests that the formation of porous structure of the composite silica-titania during the post-synthetic is similar to the observed for the pure SiO_2, which is due to the suppression of the TiO_2 crystal growth and high degree of titania species dispersion within the silica matrix.

3.2 Thermoanalytical study

The prepared porous spherical particles thermally treated at 400 ºC, in order to eliminate adsorbed ammonia and unreacted precursor species, have been subjected to thermoanalytical study. It shows that the mass loss observed for T400 is inferior to that of ST400, also the position of the endothermic effect related to the elimination of physically adsorbed and chemically bonded water is found to be displaced at higher

temperatures for ST400 than for T400 (Fig. 4). These observations indicate the fact that larger amount of water is retained in the composite material either due to its microporous structure or to its different chemical composition. The exothermic effect found on the DSC curve of the ST400 sample near 650 ºC is most likely to be attributed to the transition of amorphous titania to crystalline anatase (Fig. 4). The absence of the similar effect on the DSC curve of T400 is clearly explained by its crystalline nature [31].

3.3 Powder XRD study

The PXRD patterns of the prepared composites registered at different treatment temperatures show that the silica-titania samples are amorphous if treated at temperatures up to 400 ºC (Fig. 5). Crystalline TiO_2 anatase phase only appears after the material is heated to 700 ºC (Fig. 5), which is in agreement with the thermoanalytical data discussed above (Fig. 4). Therefore, the process of TiO_2 crystallization is strongly hindered because of the dispersion of TiO_2 into the SiO_2 matrix. The retardation of the titania crystal growth up to high temperatures might be advantageous for application of such material in catalytic or adsorption processes due to high dispersion of active titania species [1-7]. Contrary to that, the TiO_2 prepared with the use of the same synthetic method is already crystalline after the post-synthetic treatment (Fig. S5, Table S2) [31].

3.4 Spectroscopic studies

Mutual dispersion of the two oxides is apparent from the FTIR analysis. The FTIR absorption spectra of the both composites and the reference Stöber silica show the stretching vibration of O–H bonds in the range of 3300–3700 cm^{-1}. The absorbance at 3200 cm^{-1}, which is clearly observed on the spectrum of the ST50 sample most probably derives from the superposition of vibrations of adsorbed H_2O molecules and N–H stretching vibrations corresponding to the presence of ammonia in the silica-titania samples untreated under high temperatures (Fig. 6). The bending modes of O–H groups manifest themselves at 1634 cm^{-1}, while the bending vibrations of N–H bonds in the adsorbed ammonia are found at 1402 cm^{-1} only for the T50 and ST50 samples (Figs. 6 and S6). Asymmetric stretching vibrations of the Si–O–Si bonds in the pure silica are proved by the absorbance at 1108 cm^{-1} with a shoulder at 1200 cm^{-1} (Fig. 6). The introduction of titania

species into the silica matrix may cause formation of a small number of tetracoordinated TiO_x units, and it also provokes the distortion of SiO_4 tetrahedra. The shift of the absorption maximum, corresponding to asymmetric stretching vibrations of Si–O–Si, to lower wavenumbers is a clear indication of the incorporation of heteroatoms inside the silica structure (Fig. 6). The absorption at 940–960 cm^{-1} can be attributed to the vibration of Si–OH groups or Si–O–Ti linkages. Usually the intensity of the peak corresponding to silanol groups in pure silica is relatively low, as it is seen from the spectrum of Stöber SiO_2; contrary to that, the relative intensity of the peak in this region with respect to that of asymmetric stretching of Si–O–Si is significantly higher for the composite (Fig. 6), which tells us that the proper assignation of this peak would be to Si–O–Ti bonds vibration. Another important feature revealed by the FTIR spectroscopy is the presence of absorbance at about 800 cm^{-1} on the spectrum of Stöber SiO_2 corresponding to symmetric stretching vibrations of Si–O ring structure (Fig. 6). The incorporation of heteroatoms into the silica matrix distorts its structure making the absorbance of IR in this region to disappear, thus the absence of the peak at about 800 cm^{-1} or its low intensity is a fingerprint feature showing the homogeneous distribution of titania inside the composite [33]. The absorbance at 800 cm^{-1} cannot be seen on the spectrum of ST50, while it can be distinguished in the case of ST400 sample demonstrating partial segregation of the composite's constituents caused by thermal treatment (Fig. 6).

The XPS method demonstrates that the surface atomic ratio of Si/Ti is different from that in the bulk of the silica-titania spheres (Table 2). Similar observations were reported in our earlier study on the nonporous SiO_2-TiO_2 spherical particles [29]. On the presented XPS spectra of O1s region it is possible to distinguish three major contributions with energies of 530.4–530.6, 532.0 and 532.9 eV, corresponding to the oxygen of Ti–O–Ti, Si–O–Ti, and Si–O–Si bonds, respectively [34] (Fig. 7). It is clearly seen that thermal treatment of the silica-titania microporous spheres up to 400 ºC does not provoke complete segregation of the mixed oxides and the Si–O–Ti heterolinkages are still present (Fig. 7.). The decrease of the contribution at 532.9 eV is most likely to be due to the elimination of adsorbed and chemically bonded water, which normally reveals itself on the XPS O1s spectrum at binding energies higher than 533 eV [35].

3.5 TEM observations

The TEM images of the microporous silica-titania spheres dried at 50 °C after being synthesized show that the particles possess the regular spherical shape (Fig. 8a). Higher magnification reveals the presence of the surface "spike–like" structures with sizes of about 10 nm (Fig. 8b,c). The presence of crystalline phases is not evidenced by the HRTEM micrographs (Fig. 8), which is in full agreement with the selective area electron diffraction (SAED) data, where also no reflections of a crystalline phase are observed (Fig. 8d). Particle sizes vary in the range from 300 to 1300 nm, and they are represented on the histogram, showing the mean size to be 750 nm (Fig. S7a). According to the STEM-EDX analysis the elements constituting silica-titania samples are uniformly distributed, while Si/Ti atomic ratio is close to equimolar, being in fact equal to 1.18 (Fig. 8e).

Calcination of the microporous silica-titania at 400 ºC causes slight shrinkage of the spheres down to the mean size of 690 nm (Fig. 9a,b). Size distribution of the calcined particles shifts accordingly to the range of 200 to 1200 nm with the maximum at approximately 600 nm (Fig. S7b). On the basis of the HRTEM micrographs one can see that the "spike–like" structures are still present on the surface, and only they are found to be present in the crystallized state, while the rest of the particle is amorphous (Fig. 9c). The SAED pattern supports this observation showing no reflections of any crystalline phase coming from the bulk of the spheres (Fig. 9d). Elemental mapping shows uniform distribution of Si and Ti in the bulk of the microporous composite (Fig. 9e), allowing us to confirm that no major segregation of phases takes place during the process of calcination.

3.6 Point of zero charge determination

The surface potential of adsorbents shows the range of the pH values where material has its surface positively or negatively charged. Knowing the value of PZC helps to choose the optimal pH range for metal cations uptake by the adsorbent. The plot of zeta potentials versus pH values of the sample suspensions shows the reduction of PZC for the silica-titania composite to 3.1 with respect to that of pure titania, which has PZC equalling 4.1 (Fig. 10). This is in accordance with the data described in the literature, where PZC of composite SiO_2-TiO_2 [36] was found to be lower than that of pure titania [34]. The incorporation of TiO_2 into the matrix of SiO_2 causes a shift of PZC towards that of pure SiO_2, which is known to be usually in the range from 1.5 to 2.5 [37].

3.7 Lead adsorption on TiO_2 and SiO_2-TiO_2

It has been established that the process of adsorption is fast enough as the equilibrium is reached within 1 h (Fig. S8). The pure SiO_2 samples show significantly reduced adsorption capacity toward Pb^{2+} ions than other materials (Fig. S9). The T50 and ST50 samples exhibit the highest adsorption capacities due to their large SSA, developed microporosity and, probably, the ion-exchange process occurring between the Pb^{2+} ions of the solution and the surface protons of hydroxyls and amino-groups (Fig. 11). After calcination at 400 ºC their adsorption capacity drops dramatically, but T400 still adsorbs 4 times as much of Pb^{2+} on the unit of its surface than ST400 does (Table S3). Higher specific adsorption capacities of TiO_2 materials in comparison with SiO_2-TiO_2 hardly can be attributed to the ion exchange process between ammonium ions attached to the surface of the adsorbents and the Pb^{2+} ions of the solution, because ammonium ions are not detected on the FTIR spectra after calcination at 400 °C (Fig. 6). Superior specific adsorption capacity of TiO_2 spheres is probably related to its larger pore size in comparison to that of SiO_2-TiO_2 treated under the same conditions. Taking into account the size of hydrated Pb^{2+} ion, which is equal to 4.01 Å [38], one may assume that a significant part of micropores of ST400 are excluded from the adsorption process. On the other hand, the mesopores of T400 are completely accessible for Pb^{2+} ions. Increased adsorption of divalent cations on TiO_2 relative to that of SiO_2 is well known and attributed to higher energy of ion adsorption on TiO_2 [26,39]. Further increase of calcination temperature results in crystal growth of TiO_2 anatase in the pure titania [31], as well as in the transition of amorphous titania contained in the SiO_2-TiO_2 into the crystalline state, thus provoking the SSA decrease and collapse of microporous structure. Hence, the adsorbents calcined at 700 ºC demonstrate negligible uptake of lead ions (Fig. 11).

In order to elucidate the adsorption mechanism, two models were compared. First, the Langmuir isotherm model, which considers irreversible adsorption on a monolayer, while the interaction forces between the adsorbate molecules and their mobility along the surface are negligible (Table 3). The second model applied to treating the obtained data was the Freundlich model. It proposes the heterogeneous surfaces where adsorptive sites have different energy (Table 4).

The Langmuir approximation (Fig. 11A) reveals that the model of monolayer adsorption fits better than the Freundlich model to all adsorbents with an exception of T50. Dimensionless constant R_L, which indicates

whether the adsorption process is favorable, has its value in the range $1 > R_L > 0$, thus pointing to the favorability of physisorption. On the contrary, the Freundlich approximation describes the T50 isotherm well but shows worse fit than the Langmuir model does for all other adsorption isotherms (Fig. 11B). The Freundlich n-constant invariably points to favourable adsorption ($10 > n > 1$). Therefore, it may be suggested that adsorption follows the monolayer mechanism in all cases except for the T50 material. For this sorbent the presence of adsorption sites with different energies of adsorption is possible. As we know from the N_2 adsorption studies of the T50 material, it has significant volumes of micro- as well as mesopores. Consequently, the adsorption energy inside the pores of different sizes may vary significantly. Other samples predominantly have only one type of pores, either micro- or mesopores, and it can be assumed that these solids have adsorption sites with very similar energies.

Industrial wastewaters can differ in acidity, which influences the performance of adsorbents dramatically. In acidic media the surfaces of many metal oxide-based adsorbent materials are positively charged, hence they tend to adsorb anions rather than cations. In order to clarify this question, the pH range of 1-5 has been chosen as representative of industrial wastewaters.

The adsorption measurements for the selected samples at varying pH values show superior performance of the composite oxide in the uptake of Pb^{2+} in acidic conditions (Fig. 12), which is explained by its reduced PZC caused by the incorporation of TiO_2 into the silica matrix (Fig. 10).

Adsorbents in industry must be easily recoverable and retain their adsorption capacity at high level for many adsorption cycles. For regeneration study 4 materials were chosen: T50, T400, ST50, ST400. Adsorbents calcined at 700 °C were excluded from this experiment due to their poor performance. The adsorbents retain more than 60 % of their initial capacity in 5 consecutive adsorption cycles (Fig. 13). The maximum adsorption capacities found in the present case, although below that observed for polymeric resins (appx. 300 mg g^{-1}) [27], are higher than those demonstrated by modified carbon nanotubes (13 mg g^{-1}) [28], and natural minerals (50-60 mg g^{-1}) [40]. Pure titania demonstrate superior adsorption to that of silica and silica-titania composites, however the formation of silica-titania materials has a twofold role. It allows to decrease the amount of more expensive composite constituent TiO_2 and to produce the adsorbent with enhanced Pb^{2+} adsorption in acidic solutions.

5 Conclusions

In this study, the method of preparation of microporous composite SiO_2-TiO_2 spherical particles with apparent surface area value of 500 $m^2 \cdot g^{-1}$ has been demonstrated. The composite silica-titania material is able to retain its high apparent SSA and micropore volume up to calcination temperature of 400 °C. The peroxo route implemented in this work uses stable aqueous peroxotitanate complex solution as a precursor for TiO_2, thus avoiding the application of organic ligands or TEOS pre-hydrolysis for equilibration of hydrolysis rates of titania and silica sources. Formation of the SiO_2-TiO_2 composite with high degree of mutual mixing of the constituents has been verified by STEM-EDX, FTIR, and XPS analyses. The composite SiO_2-TiO_2 oxide stays amorphous up to 600 °C due to the incorporation of TiO_2 into the silica matrix and the presence of Si–O–Ti heterolinkages. The prepared microporous silica-titania and micro/mesoporous pure titania materials have been tested in the removal of lead(II) ions from aqueous solution. It has been established that the pure TiO_2 possesses higher adsorption capacity than the silica-titania, although the latter is able to adsorb Pb^{2+} even in acidic conditions, which is due to its lower PZC value than that of its pure titania counterpart.

Acknowledgments. South Ural State University is grateful for financial support of the Ministry of Education and Science of the Russian Federation (grant No 16.2674.2014/K). University of Oviedo gratefully acknowledges financial support from the Spanish MINECO (MAT2013-40950-R and MAT2016-78155-C2-1-R). Igor Krivtsov thanks for the support the Russian Foundation for Basic Research 13-03-12188-ofi.

References

[1] M. Itoh, H. Hattori, K. Tanabe, The acidic properties of TiO_2-SiO_2 and its catalytic activities for the amination of phenol, the hydration of ethylene and the isomerization of butene, J. Catal. 35 (1974) 225-231.

[2] J.R. Sohn, H.J. Jang, Correlation between the infrared band frequency of the silanol bending vibration in TiO_2-SiO_2 catalysts and activity for acid catalysis, J. Catal. 132 (1991) 563-565.

[3] A. Koreniuk, K. Maresz, K. Odrozek, J. Mrowiec-Białoń, Titania-silica monolithic multichannel microreactors. Proof of concept and fabrication/structure/catalytic properties in the oxidation of 2,3,6-trimethylphenol, Micropor. Mesopor. Mater. 229 (2016) 98-105.

[4] V. Boffa, L. Parmeggiani, A.H. Nielsen, G. Magnacca, Hydrophilicity and surface heterogeneity of TiO_2-doped silica materials for membrane applications, Micropor. Mesopor. Mater. 221 (2016) 81-90.

[5] Y. Farhang-Ghoje Biglu, E. Taheri-Nassaj, Synthesis and characterization of alumina supported microporous 3 SiO2–10 wt%TiO2 membrane for nitrogen separation, J. Industrial Engineering Chem. 19 (2013) 1752-1759.

[6] Y. Gu, S.T. Oyama, Permeation properties and hydrothermal stability of silica–titania membranes supported on porous alumina substrates, J. Membrane Sci. 345 (2009) 267–275.

[7] A. Farsi, C. Malvache, O. De Bartolis, G. Magnacca, P.K. Kristensen, M.L. Christensen, V. Boffa, Design and fabrication of silica-based nanofiltration membranes for water desalination and detoxification, Micropor. Mesopor. Mater. 237 (2017) 117–126.

[8] R.B. Greegor, F.W. Lytle, D.R. Sandstrom, J. Wong, P. Schultz, Investigation of TiO_2-SiO_2 glasses by X-ray absorption spectroscopy, J. Non-Cryst. Solids 55 (1983) 27-43.

[9] M.R. Backer, R. Cavender, M.L. Elder, P.C. Jones, J.A. Murphy, Method of manufacturing optical waveguide fiber with titania-silica outer cladding. U.S. Patent Number 5,067,975 (1991).

[10] J. Ren, S. Liu, Z. Li, X. Lu, K. Xie, Oxidative carbonylation of methanol to dimethyl carbonate over $CuCl/SiO_2$–TiO_2 catalysts prepared by microwave heating: the effect of support composition, Appl. Catal. A: General 366 (2009) 93–101.

[11] C.U.I. Odenbrand, J.G.M. Brandin, G. Busca, Surface acidity of silica-titania mixed oxides, J. Catal. 135 (1992) 505-517.

[12] E.I. Ko, J.P. Chen, J.G. Weissman, A study of acidic titania/silica mixed oxides and their use as supports for nickel catalysts, J. Catal. 105 (1987) 511-520.

[13] J.N. Hay, H.M. Raval, Synthesis of organic-inorganic hybrids via the non-hydrolytic sol-gel process, Chem. Mater. 13 (2001) 3396-3403.

[14] N. Hüsing, B. Launay, D. Doshi, G. Kickelbick, Mesostructured silica-titania mixed oxide thin films, Chem. Mater. 14 (2002) 2429–2432.

[15] M. Schraml-Marth, K.I Walther, A. Wokaun, B.E. Handy, A. Baiker, Porous silica gels and TiO_2/SiO_2 mixed oxides prepared via the sol-gel process: characterization by spectroscopic techniques, J. Non-Cryst. Solids 143 (1992) 93-111.

[16] S. Vives, C. Meunier, Influence of the synthesis route on sol–gel SiO_2–TiO_2 (1:1) xerogels and powders, Ceram. Inter. 34 (2008) 37–44.

[17] W. Li, D. Zhao, Extension of the Stöber method to construct mesoporous SiO_2 and TiO_2 shells for uniform multifunctional core-shell structures, Adv. Mater. 25 (2013) 142-149.

[18] Q. Shen, H.Y. Cheung, TiO_2/SiO_2 core−shell composite-based sample preparation method for selective extraction of phospholipids from shrimp waste followed by hydrophilic interaction chromatography coupled with quadrupole time-of-flight / mass spectrometry snalysis, J. Agric. Food Chem. 62 (2014) 8944−8951.

[19] R.S. Pillai, S.A. Peter, R.V. Jasra, Adsorption of carbon dioxide, methane, nitrogen, oxygen and argon in NaETS-4, Micropor. Mesopor. Mater. 113 (2008) 268–276.

[20] F. Yazdanbakhsh, M. Bläsing, J.A. Sawada, S. Rezaei, M. Müller, S. Baumann, S.M. Kuznicki, Copper exchanged nanotitanate for high temperature H_2S adsorption, Ind. Eng. Chem. Res. 53 (2014) 11734−11739.

[21] G. Gürboğa, H. Tel, Y. Altaş, Sorption studies of cesium on TiO_2–SiO_2 mixed gel spheres, Sep. Purif. Technol. 47 (2006) 96–104.

[22] W. Stöber, A. Fink, Controlled growth of monodisperse silica spheres in the micron size range, J. Colloid Interface Sci. 26 (1968) 62–69.

[23] J.H. Pan, Q. Wang, D.W. Bahnemann, Hydrous TiO_2 spheres: an excellent platform for the rational design of mesoporous anatase spheres for photoelectrochemical applications, Catal. Today, 230 (2014) 197-204.

[24] J. Sekulić, J. E. ten Elshof, D.H.A. Blank, A microporous titania membrane for nanofiltration and pervaporation, Adv. Mater. 16 (2004) 1546–1550.

[25] E.N. Coker, Inorganic Ion Exchangers, BP Amoco Chemicals, Sunbury-on-Thames, Middlesex, UK (2000) Academic Press, p.1564.

[26] R.O. James, T.W. Healy, Adsorption of hydrolyzable metal ions at the oxide-water interface. I. Co(II) adsorption on SiO_2 and TiO_2 as model systems, J. Colloid Interface Sci. 40 (1972) 42-52.

[27] A. Hosseini-Bandegharaei, R. Khamirchi, R. Hekmat-Shoar, A. Rahmani-Sani, A. Rastegar, Z. Pajohankia, E. Fattahi, Sorption efficiency of three novel extractant-impregnated resins containing vesuvin towards Pb(II) ion: effect of nitrate and amine functionalization of resin backbone, Coll. Surf. A-Physicochem. Eng. Aspect, 504 (2016) 62-74.

[28] T.A. Saleh, Nanocomposite of carbon nanotubes/silica nanoparticles and their use for adsorption of Pb(II): from surface properties to sorption mechanism, Desalin. Water Treat., 57(2015) 10730-10744.

[29] R. Morozov, I. Krivtsov, V. Avdin, Z. Amghouz, S.A. Khainakov, J.R. García, Peroxo method for preparation of composite silica–titania spheres, J. Non-Cryst. Solids, 435 (2016) 8–16.

[30] I. Krivtsov, M. Ilkaeva, V. Avdin, Z. Amghouz, S.A. Khainakov, J.R. García, E. Díaz, S. Ordóñez, Exceptional thermal stability of undoped anatase TiO_2 photocatalysts prepared by a solvent-exchange method, RSC Adv. 5 (2015) 36634-36641.

[31] M. Ilkaeva, I. Krivtsov, E. Díaz, Z. Amghouz, Y. Patiño, S. Khainakov, J.R. García, S. Ordóñez, Photocatalytic degradation of 2-(4-methylphenoxy)ethanol over TiO_2 spheres, J. Hazard. Mater. 332 (2017) 59-69.

[32] M. Thommes, K. Kaneko, A.V. Neimark, J.P. Olivier, F. Rodriguez-Reinoso, J. Rouquerol, K.S.W. Sing, Physisorption of gases, with special reference to the evaluation of surface area and pore-size distribution (IUPAC Technical Report), Pure Appl. Chem. 2015.

[33] I.V. Krivtsov, M.V. Ilkaeva, V.V. Avdin, D.A. Zherebtsov, Properties and segregation stability of the composite silica-zirconia xerogels prepared via "acidic" and "basic" precipitation routes, J. Non-Cryst. Solids, 362 (1) (2013) 95-100.

[34] H.S. Kibombo, R. Peng, S. Rasalingam, R.T. Koodali, Versatility of heterogeneous photocatalysis: synthetic methodologies epitomizing the role of silica support in TiO_2 based mixed oxides, Catal. Sci. Technol. 2 (2012) 1737–1766.

[35] A. Verdaguer, C Weis, G. Oncins, G. Ketteler, H. Bluhm, M. Salmeron, Growth and Structure of Water on SiO_2 Films on Si Investigated by Kelvin Probe Microscopy and in Situ X-ray Spectroscopies, Langmuir, 23 (2007) 9699-9703

[36] A.A. Ismail, A.A. El-Midany, I.A. Ibrahim, H. Matsunaga, Heavy metal removal using SiO_2-TiO_2 binary oxide: experimental design approach, Adsorption 14 (2008) 21-29.

[37] R.K. Iler, The Chemistry of Silica, Wiley, New York, 1979.

[38] A. Sharma, B.K. Lee, Cd(II) removal and recovery enhancement by using acrylamide–titanium nanocomposite as an adsorbent, Appl. Surf. Sci. 313 (2014) 624–632.

[39] K. Bourikas, C. Kordulis, J. Vakros, A. Lycourghiotis, Adsorption of cobalt species on the interface, which is developed between aqueous solution and metal oxides used for the preparation of supported catalysts: a critical review, Adv. Colloid Interface Sci. 110 (2004) 97–120.

[40] M. Hamidpour, M. Kalbasi, M. Afyuni, H. Shariatmadari, P.E. Holm, H.C.B. Hansen, Sorption hysteresis of Cd(II) and Pb(II) on natural zeolite and bentonite, J. Hazard. Mater. 181 (2010) 686-691.

Figure Captions

Figure 1. SEM images of non-calcined (a) pure TiO_2 spheres and (b) composite SiO_2-TiO_2 spheres.

Figure 2. N_2 adsorption-desorption isotherms of the porous composite SiO_2-TiO_2 spheres.

Figure 3. Micropore size distribution of the porous composite SiO_2-TiO_2 spheres.

Figure 4. Thermoanalytical study of porous titania and silica-titania spheres subjected to calcination at 400°C.

Figure 5. PXRD patterns of the composite SiO_2-TiO_2 spheres.

Figure 6. FTIR spectra of the composite SiO_2-TiO_2 spheres.

Figure 7. XPS spectra of O1s region.

Figure 8. (a-c) TEM images of the ST50 sample, (d) SAED pattern, and (e) STEM images of mapping of elements distribution: Ti (red), Si (green), O (blue).

Figure 9. (a-c) TEM microphotograph of the ST400 sample, (d) SAED pattern, and (e) STEM images of mapping of elements distribution: Ti (red), Si (green), O (blue).

Figure 10. PZC determination of the T400 and ST400 samples.

Figure 11. Isotherms of Pb^{2+} adsorption.

Figure 12. Capacity of Pb^{2+} adsorption in relation to the solution pH values.

Figure 13. Regeneration of the adsorbents.

Figures

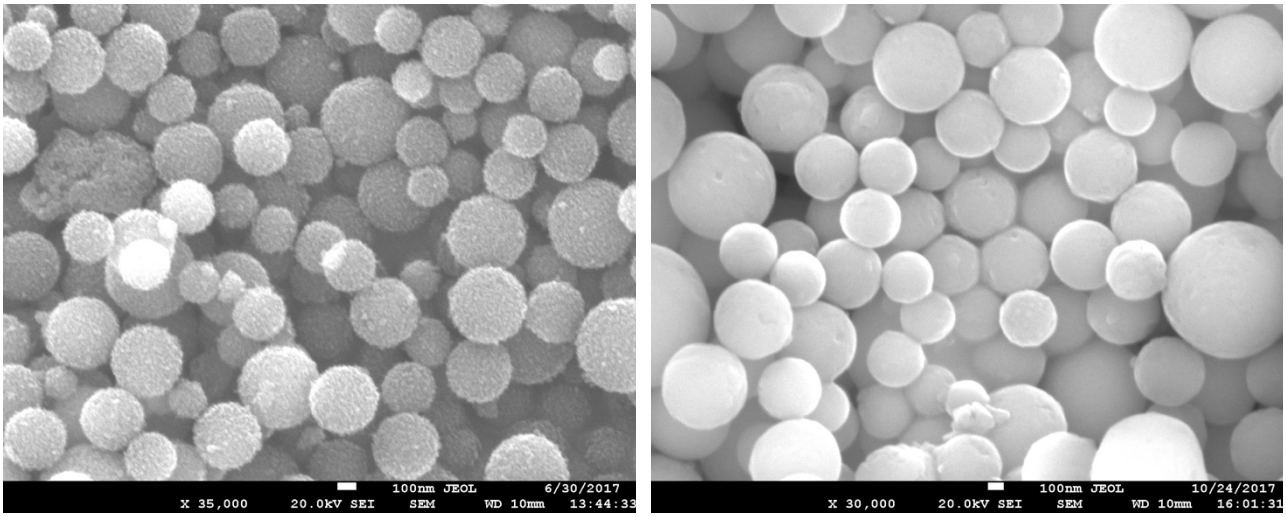

a **b**

Fig. 1

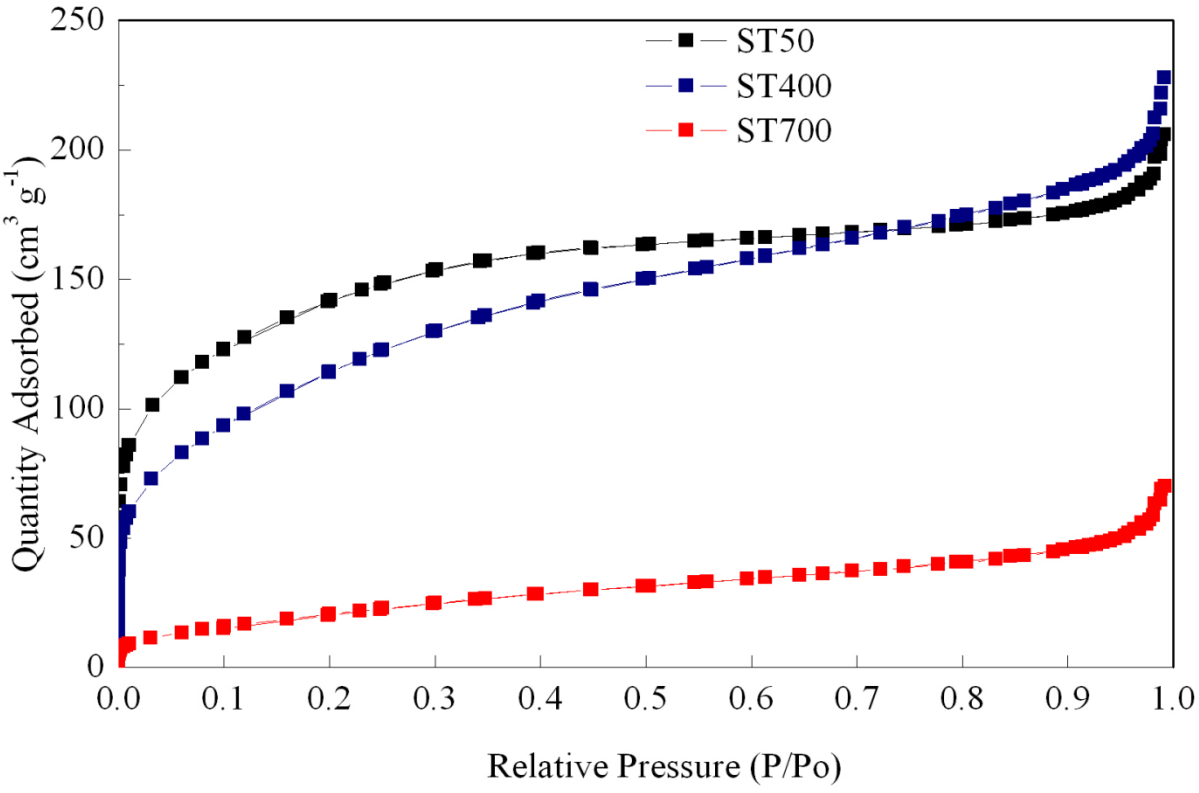

Fig. 2

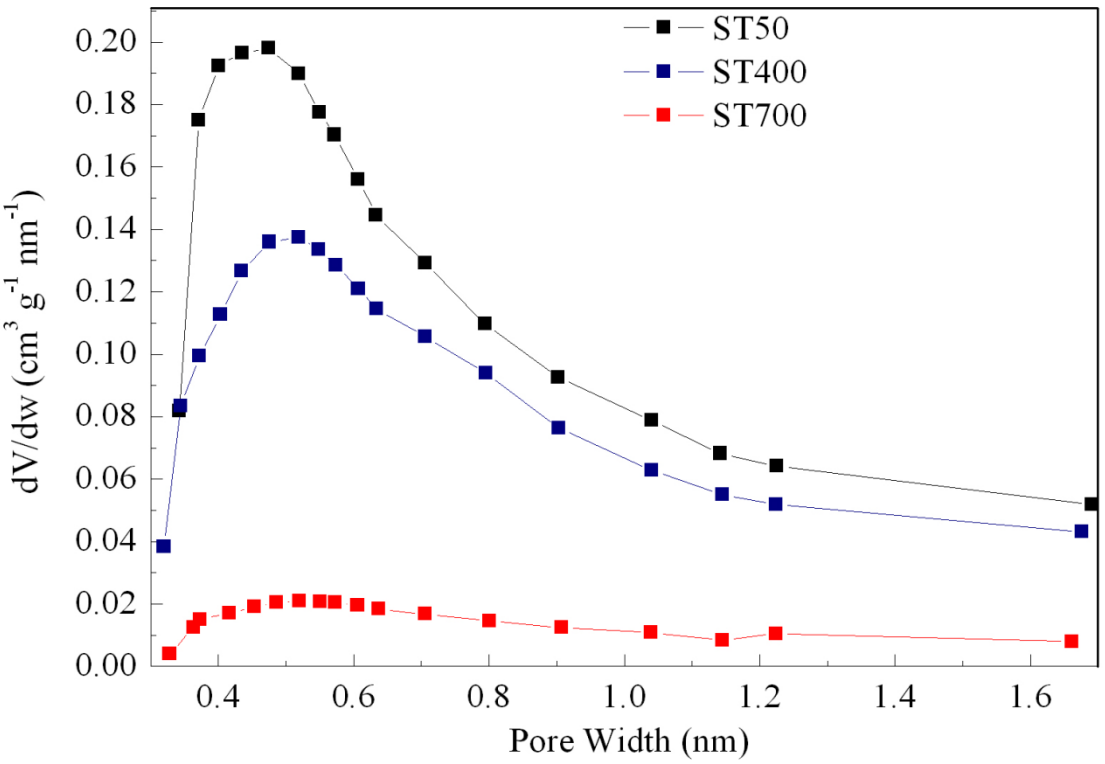
ST50
ST400
ST700
dV/dw (cm^3 g^{-1} nm^{-1})
Pore Width (nm)
0.00
0.02
0.04
0.06
0.08
0.10
0.12
0.14
0.16
0.18
0.20
0.4
0.6
0.8
1.0
1.2
1.4
1.6

Fig. 3

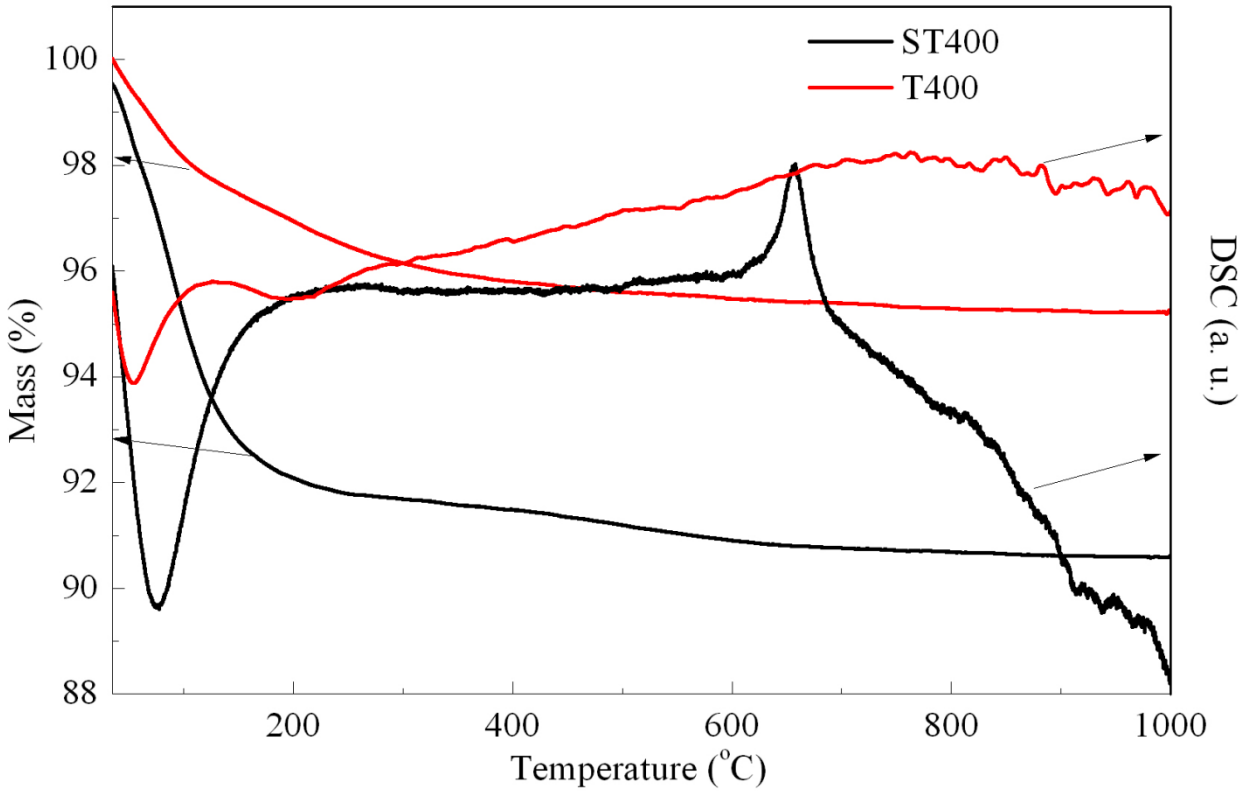
ST400
T400
Mass (%)
DSC (a. u.)
Temperature (°C)
88
90
92
94
96
98
100
200
400
600
800
1000

Fig. 4

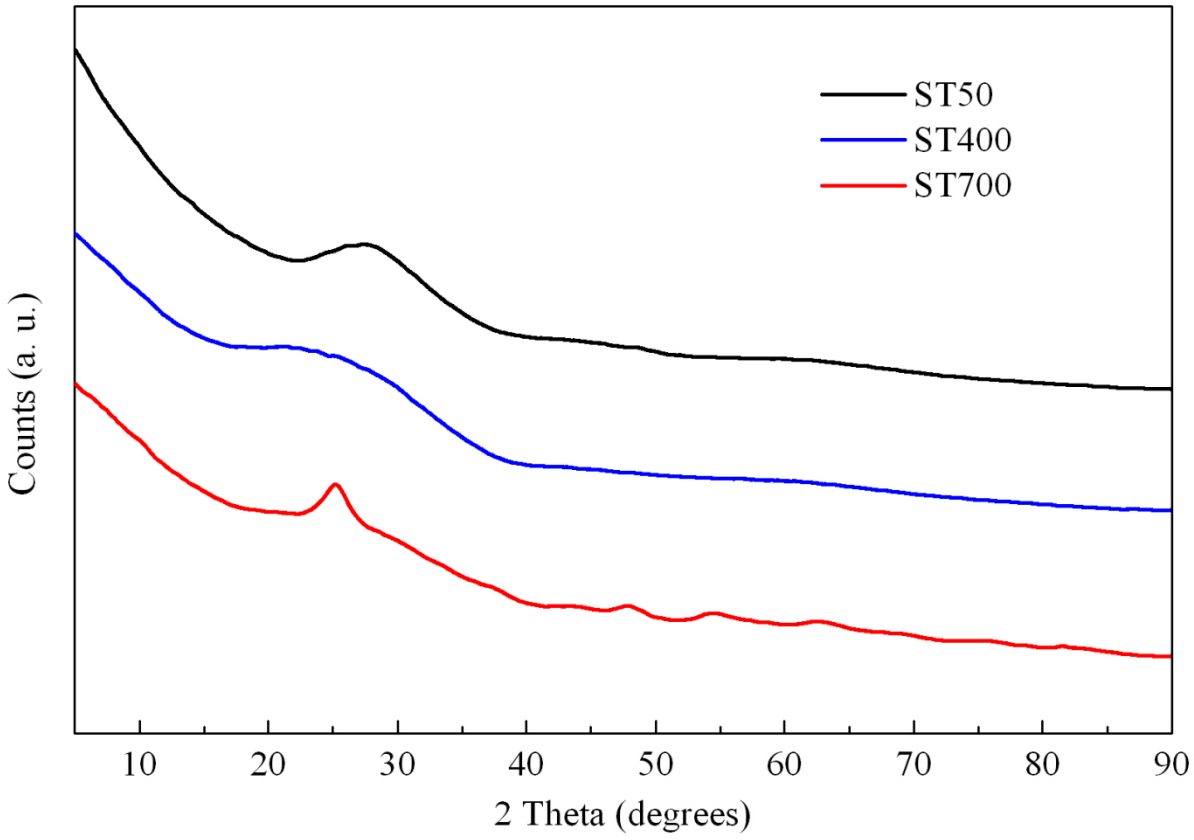
ST50
ST400
ST700
Counts (a. u.)
10
20
30
40
50
60
70
80
90
2 Theta (degrees)

Fig. 5

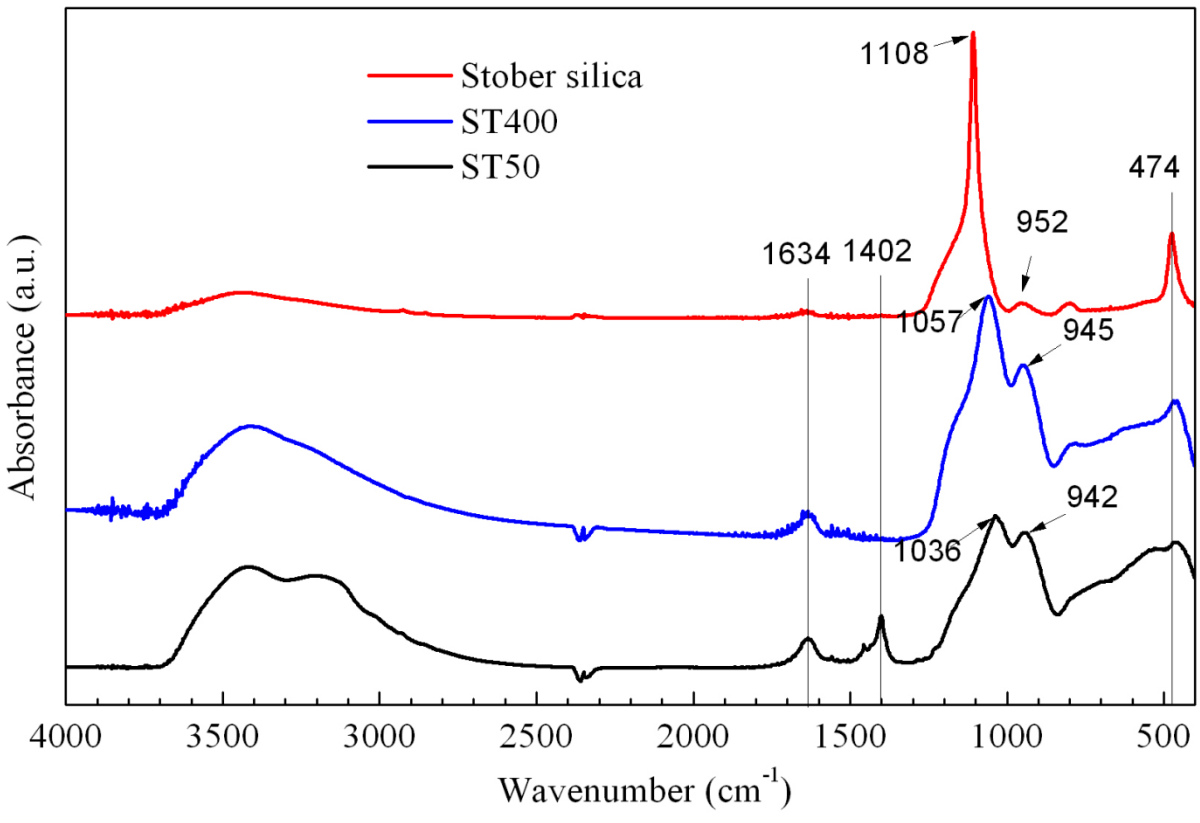
Stober silica
ST400
ST50
1108
474
952
1634
1402
1057
945
942
1036
Absorbance (a.u.)
4000
3500
3000
2500
2000
1500
1000
500
Wavenumber (cm-1)

Fig. 6

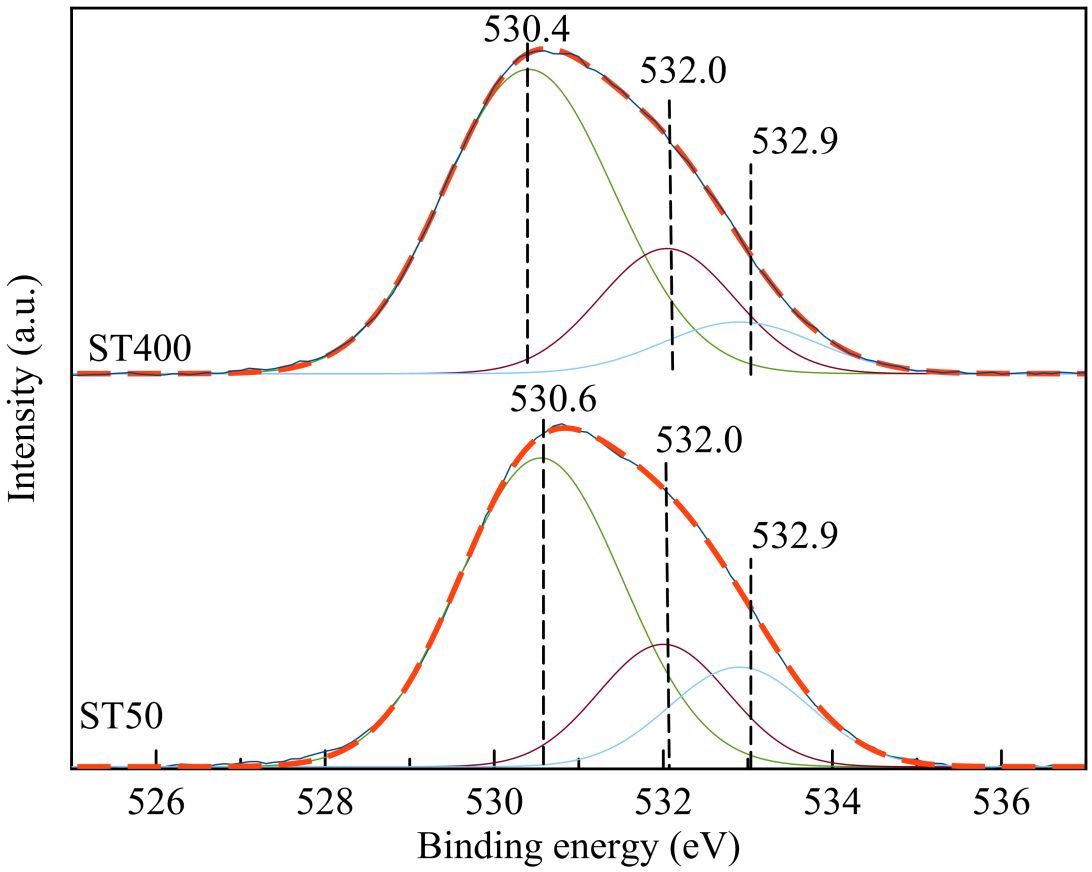
530.4
532.0
532.9
ST400
530.6
532.0
532.9
ST50
Intensity (a.u.)
526
528
530
532
534
536
Binding energy (eV)

Fig. 7

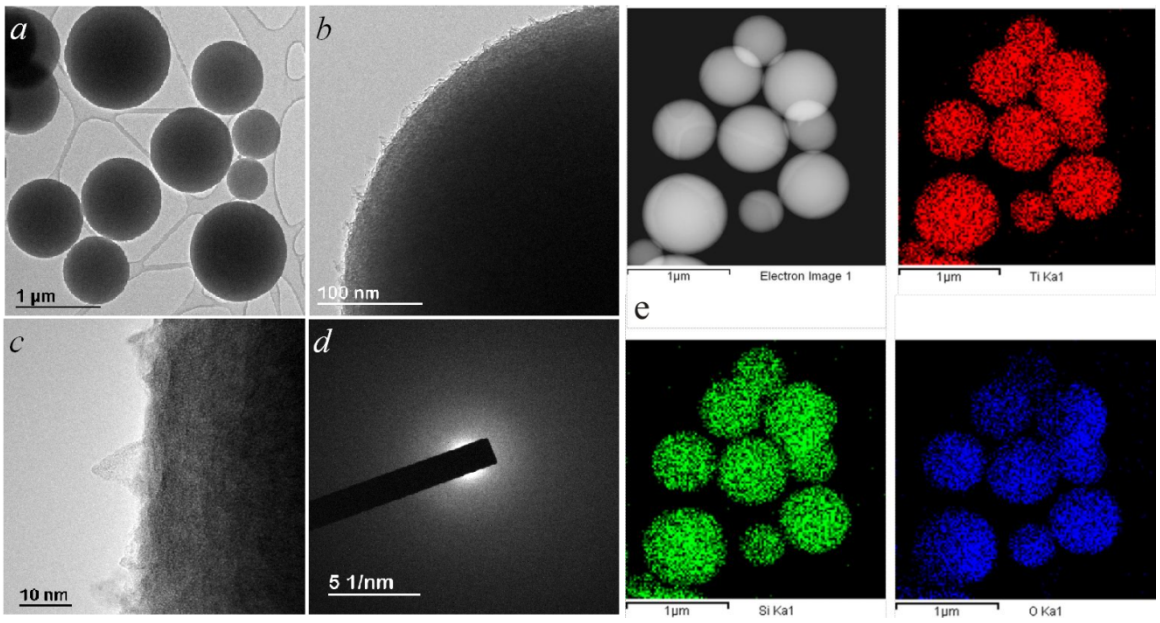
a
1 µm
b
100 nm
c
10 nm
d
5 1/nm
e
1µm
Electron Image 1
1µm
Ti Ka1
1µm
Si Ka1
1µm
O Ka1

Fig. 8

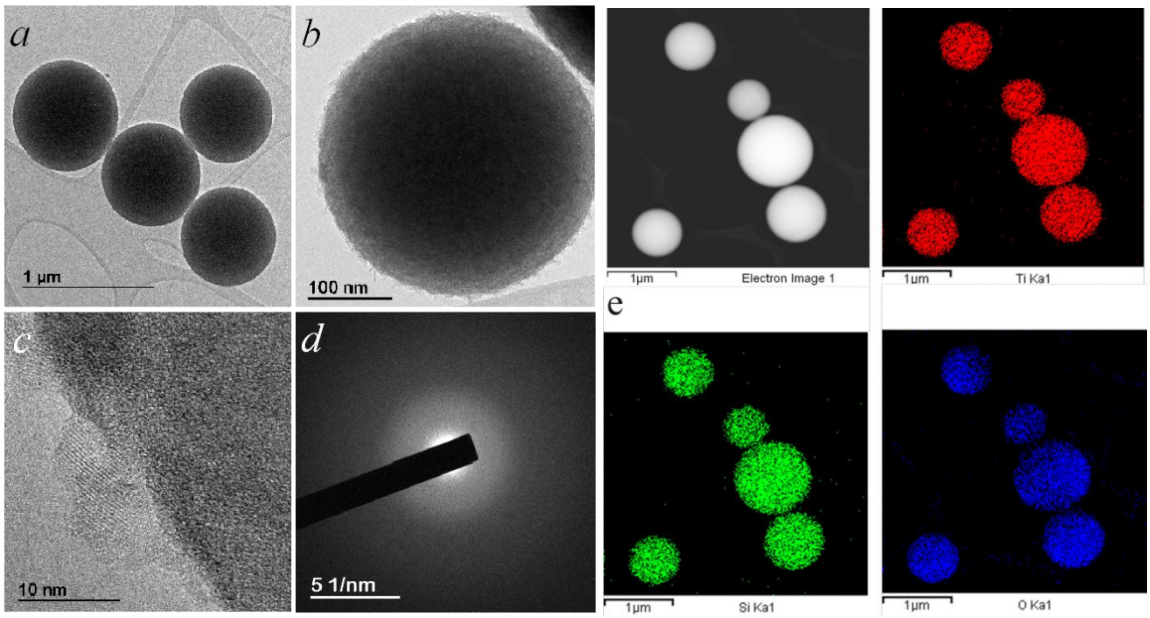
a
1 μm
b
100 nm
c
10 nm
d
5 1/nm
e
1μm
Electron Image 1
1μm
Ti Ka1
1μm
Si Ka1
1μm
O Ka1

Fig. 9

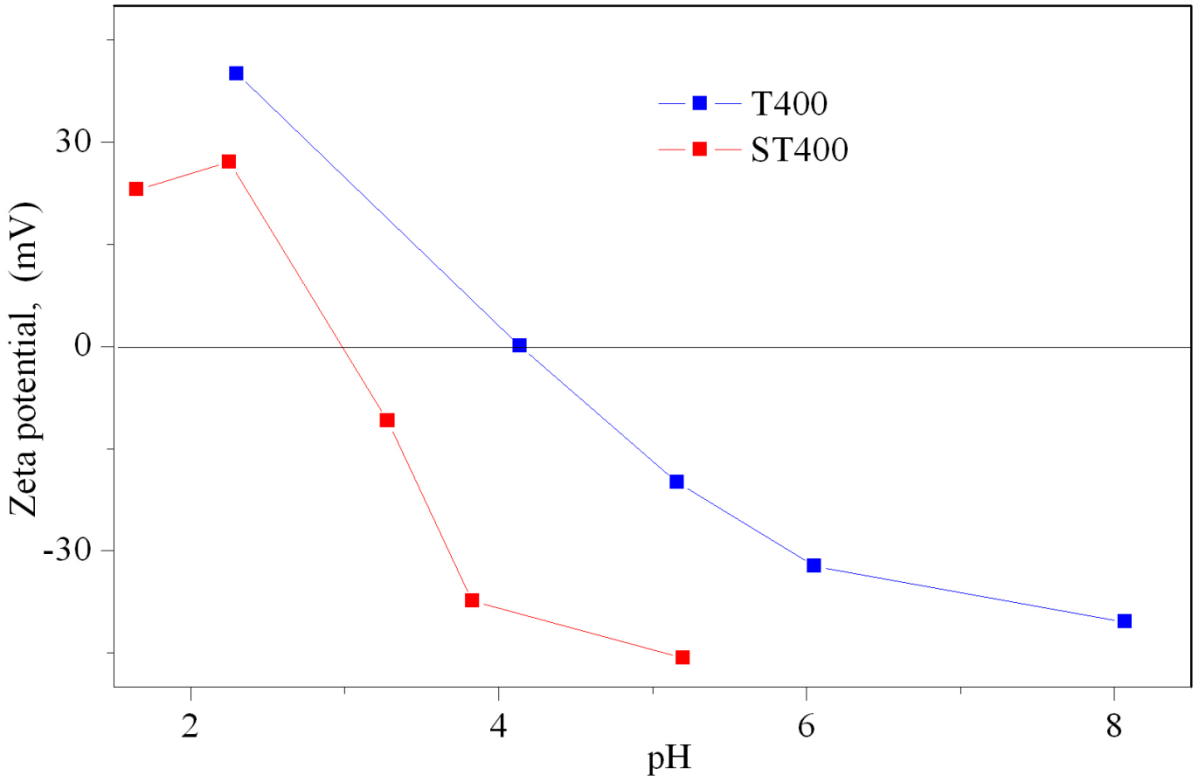
T400
ST400
Zeta potential, (mV)
30
0
-30
2
4
6
8
pH

Fig. 10

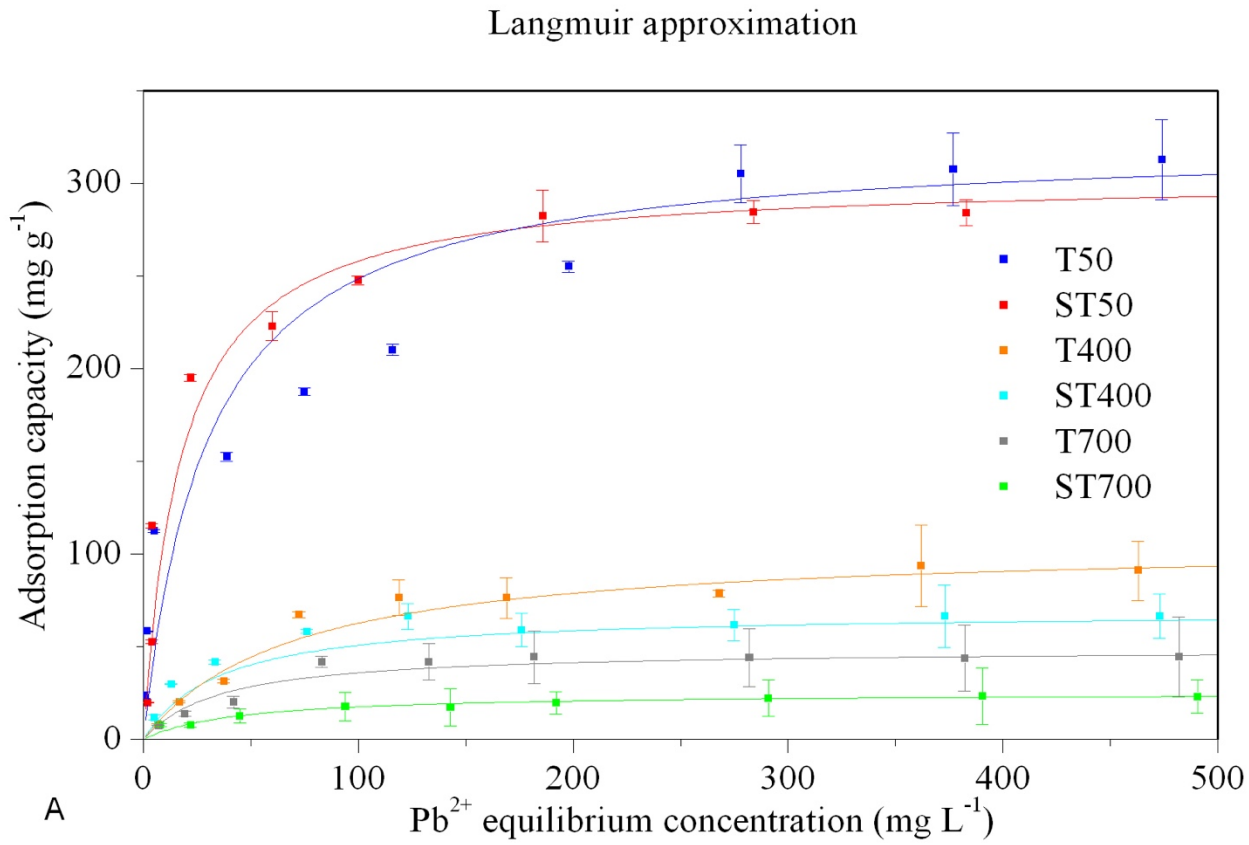
Langmuir approximation
Adsorption capacity (mg g-1)
Pb2+ equilibrium concentration (mg L-1)
T50
ST50
T400
ST400
T700
ST700
A

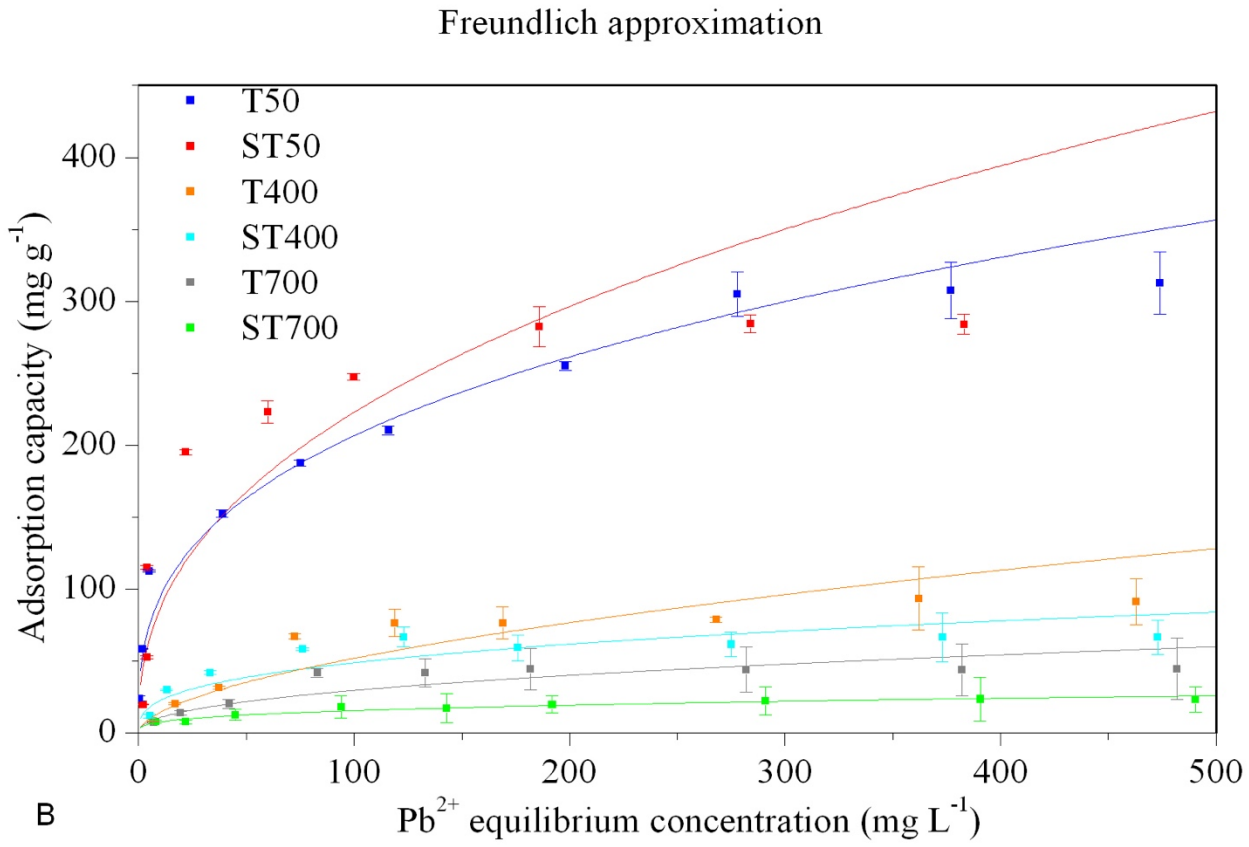
Freundlich approximation
Adsorption capacity (mg g-1)
Pb2+ equilibrium concentration (mg L-1)
T50
ST50
T400
ST400
T700
ST700
B

Fig. 11

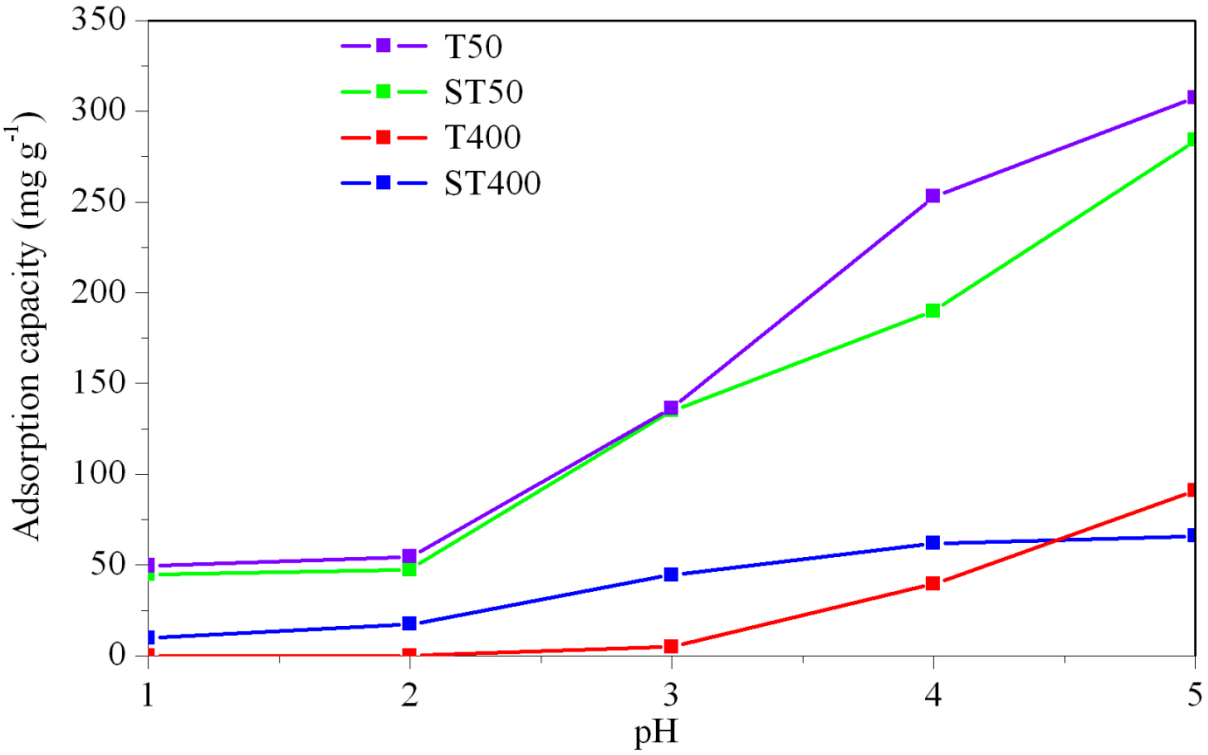
T50
ST50
T400
ST400
Adsorption capacity (mg g-1)
pH
0
50
100
150
200
250
300
350
1
2
3
4
5

Fig. 12

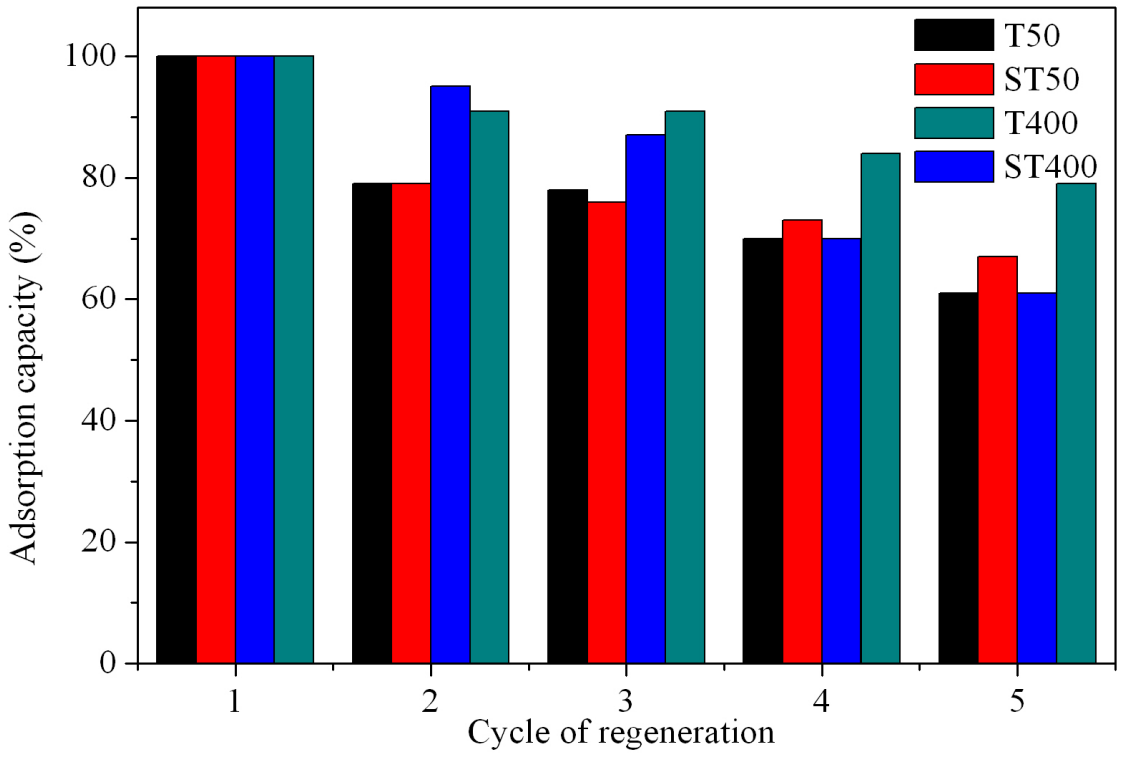
T50
ST50
T400
ST400
Adsorption capacity (%)
Cycle of regeneration
0
20
40
60
80
100
1
2
3
4
5

Fig. 13

Tables

Table 1. Apparent SSA and pore volumes of the composite SiO_2-TiO_2 samples.

Sample name	Apparent BET SSA ($m^2 \cdot g^{-1}$)	C parameter value	T-plot external surface area ($m^2 \cdot g^{-1}$)	Dubinin-Astakhov micropore volume ($cm^3 \cdot g^{-1}$)
ST non porous [29]	16	67	16	-
ST50	503	194	93	0.170
ST400	418	70	176	0.140
ST700	81	33	67	0.020

Table 2. XPS surface composition of the silica-titania spheres.

Sample	Surface atomic composition	Si/Ti ratio
ST50	$Si_{20.5}Ti_{14.1}O_{65.4}$	1.45
ST400	$Si_{21.1}Ti_{14.2}O_{64.6}$	1.49

Table 3. Parameters of the Langmuir adsorption model

Sample	Maximum Langmuir sorption capacity Q_m ($mg \cdot g^{-1}$)	Langmuir equilibrium constant K ($L \cdot mg^{-1}$)	R_L	Correlation coefficient R^2
ST50	303	0.057	0.044	0.9975
ST400	69	0.051	0.040	0.9973
ST700	25	0.023	0.082	0.9935
T50	323	0.033	0.074	0.9834
T400	106	0.014	0.131	0.9863
T700	49	0.028	0.069	0.9914

Table 4. Parameters of the Freundlich adsorption model.

Sample	Freundlich coefficient Kf $((mg\ g^{-1})(L\ mg^{-1})^{1/n})$	Freundlich constant n	Correlation coefficient R^2
ST50	301	2.430	0.7739
ST400	62	2.963	0.8221
ST700	19	3.180	0.9351
T50	264	2.948	0.9477
T400	78	1.778	0.9060
T700	41	2.267	0.8789